Chapter 3

Nitrogen and Oxygen Separation

After revising the literature on nitrogen and oxygen separation, we decided to use mordenite, the porous structure of which consists of one-dimensional channels, to separate the nitrogen and the oxygen (Chapter 3.1). We selected this zeolite because the cations are aparently in easily accessible positions for N_2 and O_2 molecules. Then, we studied the adsorption properties on various cation exchanged (Na^+, Li^+, Ag^+) mordenites with different electronic properties.

In this chapter we also study how to decrease the shielding that framework walls produce on the cations. The shielding decreases the charge location on the cation and indeed disfavours the conditions for quadrupolar interaction between cations and N_2 and O_2 molecules. We therefore studied the introduction of F atoms into the zeolitic structure and the shielding effect in different cations for the N_2 and O_2 adsorption.

We also studied the incorporation of silver cations into the zeolite structure and their activation in conditions that favour the nitrogen/oxygen separation in zeolite X. After seeing the potential of mordenite as an adsorbent for nitrogen and oxygen separation, in the second part of this chapter (chapter 3.2), we attempted to form Ag_m^{n+} clusters inside the mordenite structure in order to study their adsorption properties. However, and probably because the Si/Al ratio was higher than that of zeolite X, we were not able to form these clusters

in the mordenite channels. So we performed the nitrogen and oxygen adsorption experiments on silver-exchanged zeolite A, with a Si/Al ratio around 1.

The formation of silver clusters inside zeolite A has been extensively studied; however, its adsorption properties have hardly been tested. Therefore, we formed these clusters on zeolite A and studied their nitrogen and oxygen adsorption properties as a function of the temperature used for their formation.

3.1. Study of the influence of several mordenite modifications on its N_2 and O_2 adsorption properties*

Abstract

Na-Mordenite zeolite was cation-exchanged to obtain Li, Li/Ag and Ag-Mordenite, and treated with NH_4F to obtain Na, Li, Li/Ag-MordeniteF (1%) and Na-MordeniteF (10%). Samples were characterized by XRD, nitrogen physisorption, ^{27}Al and ^{29}Si MAS NMR, FT-IR spectroscopy and X-ray fluorescence. Special attention was given to the presence of F^- ions in the mordenite structure. Equilibrium adsorption isotherms of high purity components N_2 and O_2 were measured at 298 K. For the cation-exchanged mordenite samples, the adsorbed nitrogen volume is slightly higher than that obtained in other zeolites such as zeolite X with lower Si/Al ratio. This reveals the significant influence of the cations accessibility to the gas molecules in these adsorption processes. N_2 adsorption capacity increases in the order $Na^+ < Ag^+ < Li^+$ whereas the N_2/O_2 adsorption selectivity varies in the way $Na^+ < Li^+ < Ag^+$ for the cation-exchanged mordenite samples. In samples prepared by fluorinated treatment, the effect is different depending on the extraframework cation present. When Na^+ and Li^+ cations are present, F atoms make a decrease of the shielding caused by the walls to the cations charge resulting in an increase on the adsorption selectivity, especially at low pressures, with a slight decrease in the number of active sites. However, the effect of F to Ag^+ cations is mainly an electronegative effect, making the interaction adsorbate-adsorbent less favorable.

* Journal of Physical Chemistry B **2004**, 108 (17), 5359-5364.

3.1.1. Introduction

Separation of nitrogen and oxygen by adsorption processes has become in the latest 30 years an alternative method instead of cryogenic distillation because of the large energetic cost of the later.[1,2]

Adsorption of nitrogen and oxygen in zeolites is thermodynamically controlled and it depends on the strength of interaction between the quadrupolar moment of N_2 and O_2 molecules with extraframework cations located inside the structure.[3,4,5] The quadrupolar moment of the nitrogen is three times that of oxygen. It is well known that this separation is strongly influenced by the composition and structure of the zeolites.[6] Thus, zeolites with high aluminum content (Si/Al=1), basically A and X, have been mainly used for air separation because of their high cations content, which are responsible for the coulombic interaction.

Some of these zeolites have been already modified by cationic exchange with alkaline and alkaline earth metals to improve the nitrogen and oxygen separation.[7-11] The factors affecting the interaction are mainly effective charge, polarizing power and radius of the cation. Interestingly, when Ag^+ cations interact with N_2 and O_2 molecules the bonding is a result of two contributions: the donation of the π-bond electrons to the empty s-orbital of Ag^+ and the backdonation of the d-orbital electrons of Ag^+ to the empty antibonding π-orbitals of the N_2 and O_2 molecules.[12] Because of the electron configuration of N_2 and O_2, the interaction of Ag^+ cations with N_2 becomes more favorable than with O_2.

N_2 and O_2 interactions with zeolites of low Si/Al ratio, such as zeolite X and LSX, have been highly studied by IR spectroscopy and also quantum chemically using methods based on the density functional theory.[8,13-19] These studies show that despite their high number of extraframework cations, not all sites are

equally accessible for the interaction with N_2 and O_2 molecules.[18-19] The 3D porous structure of these zeolites is based in cavities, and only cations located in determined positions are susceptible to interact with N_2 and O_2 molecules. Then, it appears interesting to choice zeolites with porous structures with lower dimensionality where cations could be more accessible to the molecules.

Theoretical results show that extraframework cations need to have a charge of + n.0 (were n= 1, 2,...) to compensate the framework's negative charge. Theoretical calculus point that the effective charge on the cations might be reduced due to a certain shielding by partial hydration and/or by the influence of framework oxygen atoms on them.[18] Introduction of elements with less polarizability in the structure, such as fluorine, should result in an increase on the total effective charge of the extraframework cations, and, consequently, an increase of the interaction between cations and the quadrupolar moment of N_2 and O_2 molecules could be expected.

The insertion of fluorine atoms in different zeolite and clay-type structures has been widely studied.[20-25] Several authors reported changes in the structure and catalytic properties of mordenite after activation by solutions of HF, KF, NH_4F and F_2, and considerable higher catalytic activity in some reactions catalyzed by acids.[23,24]

Fluorination under mild conditions (e.g. with NH_4F solutions) could involve a certain dealumination, as reported by several authors. However, there are different proposals about the location of fluorine after treatment. Some authors have discussed two possible ways for the fluoride treatment:

$$\text{zeoliteOH} + F^- (aq) \rightarrow \text{zeoliteF} + OH^- (aq) \qquad \text{(eq. 1)}$$

$$\text{zeoliteOH} + F^- (aq) \rightarrow AlF_xOH_y \text{ zeolite} \rightarrow AlF_3 (aq) + \text{zeolite}^- \qquad \text{(eq. 2)}$$

Thus, Kowalak et al.[23,24] reported the incorporation of fluorine in the framework (eq. 1) whereas Breck et al.[25] and, subsequently, Panov et al.[20]

proposed the formation of extraframework aluminium fluoride species (eq. 2). Examining the fluorination conditions used in these studies, it seems clear that the way (eq. 2) is more favoured when using high fluorine concentrations (> 3% w/w) as well as calcining at high temperatures (> 450ºC).

No studies of fluorinated zeolites are reported for separation processes. In this work, we propose to study the N_2 and O_2 adsorption properties of mordenite. This material is the natural zeolite with the lowest Si/Al ratio (6.5 in our sample). It has a 2D structure, which, actually, works as a one dimensional channel system formed by 12-ring and 8-ring channels, leading probably to a better accessibility of the extraframework cations to the molecules of adsorbate. Besides, we want to increase the charge location of different cations (Na^+, Li^+ and Ag^+) by introducing less polarizing atoms of fluorine in the framework channels of the mordenite in order to improve its adsorption properties.

3.1.2. Experimental Section

3.1.2.1. Starting Materials

Commercial Na-Mordenite (Si/Al = 6.5, CBV 10A Lot No. 1822-50), designated as NaM, was used as starting material. It was supplied by Zeolist as hydrated powder. Its chemical composition was SiO_2/Al_2O_3 mole ratio 13 and a Na_2O weight % of 6.6. Lithium chloride (LiCl, 99 % min, Prolabo), sodium chloride (NaCl, 99 % min, Prolabo), silver nitrate ($AgNO_3$, 99.8 % min, Prolabo), ammonium chloride (NH_4Cl, 99% min, Prolabo), ammonium fluoride (NH_4F, high purity, Probus) and ammonia solution (NH_3, 28%, Prolabo) were used in the preparation of the ion-exchange solutions.

3.1.2.2. Samples preparation

The treatments used to prepare the different samples are shown in Table 1.

Table 1. Sample preparation procedures

Sample	Starting sample	Treatment
NaM		None
LiM	NaM	Three exchanges with LiCl 2.2 M for 12 hours. Vacuum filtered, washed with distilled water and dried in a furnace at 383 K overnight.
AgM	NaM	One exchange with $AgNO_3$ 1M for 12 hours protected from light. Vacuum filtered, washed and dried in a furnace at 383 K overnight.
Li/AgM	LiM	One exchange with $AgNO_3$ 0.01M for 6 hours protected from light. Vacuum filtered, washed and dried in the furnace at 383 K overnight.
NaM_xF (x= 1,10)	NaM	Repeated NH_4^+ exchange with NH_4Cl 2.2 M and calcined at 673 K for 12 hours.
	HM	In tefflon flasks by exchanging 1g of H-Mordenite with 50 mL of NH_4F 8.8 mM and 0.105 M respectively (x =1, 10). After impregnation the samples were vacuum filtered and washed with distilled water.[a]
	HMxF	Bubbling a flow of NH_3/Ar through it.
	NH_4MF_x	Cation exchanged several times with NaCl 2.2 M. Vacuum filtered and washed with distilled water until be free of chlorides, and dried in a furnace at 383 K overnight.
LiM1F	NaM1F	Several exchanges with LiCl 2.2 M. Vacuum filtered, washed and dried in the furnace at 383 K overnight.
LiAgM1F	LiM1F	One exchange with $AgNO_3$ 0.01M 6 hours protected from light. Vacuum filtered, washed and dried in the furnace at 383 K overnight.

[a] Concentrations and volumes of NH_4F were calculated in the way that the % w/w of F introduced per gram of zeolite was 1 and 10.

3.1.2.3. Characterization techniques

N_2 adsorption isotherms. Nitrogen adsorption isotherms at 77K and BET surface areas were obtained using a Micromeritics ASAP 2000 surface analyzer with a value of 0,164 nm^2 for the cross section of the nitrogen molecule. Specific surface areas were obtained from the BET equation.

Powder X-ray diffraction. Powder X-ray diffraction patterns of the samples were obtained with a Siemens D5000 diffractometer (Bragg-Brentano parafocusing geometry and vertical θ-θ goniometer) fitted with a curved graphite diffracted-beam monochromator, incident and diffracted-beam Soller slits, a 0.006º receiving slit and scintillation counter as a detector. The angular 2θ diffraction range was between 5º to 70º. The data were collected with an angular step of 0.05º at 3s per step and sample rotation. $Cu_{K\alpha}$ (1.542 Å) radiation was obtained from a copper X-ray tub operated at 40kV and 30mA. The cell parameters and cell volume values were calculated using a matching profile with TOPAS 2.0 software (Bruker AXS).

^{27}Al and ^{29}Si, MAS NMR spectra were obtained at a frequency of 400 MHz by spinning at 5 kHz. The pulse duration was 2 μs and the delay time was 5 seconds. High purity octahedral hexahydrated aluminum chloride $AlCl_3 \cdot 6H_2O$ in its solid state and silicon nitride Si_3N_4 were used as the chemical shift reference for aluminum and silicium, respectively.

DRIFTS Investigations. Infrared spectra were recorded using a FTIR Bruker Equinox 55 instrument in the frequency range of 400 to 4000 cm^{-1} with a spectral resolution of 4 cm^{-1}. A MCT detector was used. Samples mixed with KBr were placed on a DRIFT cell connected to a temperature controller. Spectra of the dehydrated samples were taken after activation at 673 K for a minimum of 4 hours under an Ar flow of 2 ml/s.

X-ray fluorescence. X-ray fluorescence was used to determine the atoms distribution maps and the Si/Al ratio of the fluorinated and non-fluorinated samples. Experiments were performed on a scanning electron microscope, JEOL JSM6400, operating at accelerating voltage of 15 kV and work distances of 15 mm. All samples were covered with a graphite layer. Accumulating time for mapping experiments was around 120 seconds.

Cation exchange capacity (CEC). Cation exchange capacity (CEC) of different samples was determined in a similar way of that proposed by Bergaya et al.[26] First, mordenite samples were exchanged with an aqueous solution of $CuSO_4$ for 6 h at room temperature. Then, the samples were centrifuged and washed with distilled water several times. The amount of Cu^{2+} exchanged was determined by UV-Visible spectroscopy at 809 nm. The CEC in meq/100g of zeolite was calculated as the difference in concentration between the starting solution and the final solution obtained after the exchange.

3.1.2.4. N_2 and O_2 adsorption measurements.

Adsorption isotherms were measured using a static volumetric system Micromeritics ASAP-2010. The gases used were high purity (99,999%) N_2 and O_2. Both gases were supplied by Carburos Metálicos.

Experiments were made using an amount of sample between 0,20 to 0,30 g. Sample was contained in a quartz cup and previously activated before the adsorption measurements at 623 K using a turbomolecular vacuum pump until a pressure lower than 1μmHg. It is known that small amounts of molecular water inside the framework of the aluminosilicates seriously affect the adsorption capacity of these materials.[27] Adsorption measurement isotherms were performed at 298 K in the range of pressures compressed between 0.05 and 760 mmHg.

3.1.3. Results and Discussion

3.1.3.1. Samples characterization

Nitrogen adsorption isotherms obtained at 77 K were classified of type I for all samples, which correspond to microporous materials, according to the BDDT classification.[28] The BET surface area of the starting sample was around 350 m^2/g. Sample modifications by cation exchange do not modify porosity and surface area results. In contrast, the fluorination of mordenite with NH_4F causes structural variations which results in a slightly increase of its meso-macro porosity (see Table 2), but it does not practically affect the isotherm shape. These results are in agreement with the dealumination detected by other techniques for these samples, as commented below.

Table 2. N_2 physisorption characterization of several samples

Sample	Surface area (m^2/g)	Microp. surface area (m^2/g)	Non-microp. surface area (m^2/g)	Microp./ Non-microp.
NaM	352	321	31	10.35
NaM1F	334	303	31	9.77
NaM10F	370	320	50	6.40

Figures 1 and 2 show the ^{27}Al and ^{29}Si MAS NMR spectra, respectively, for several samples. ^{27}Al NMR of the starting mordenite (NaM) and the low fluorinated mordenite (NaM1F) show that the aluminum is mainly tetrahedrically coordinated since only one peak at 50 ppm can be observed. However, for the highly fluorinated material (NaM10F), besides this tetrahedrical aluminum, a broad band around 0 ppm indicates the presence of some octahedrical aluminum. Therefore, fluorination in mild conditions does not cause an appreciable dealumination of the structure when the amount of

fluorine used is low (1 % w/w). This has also been suggested by Kowalak et al.[23] Otherwise, when the amount of fluorine is higher (10 % w/w) part of the tetrahedrically aluminum becomes octahedrically coordinated. This peak confirms the framework dealumination, which is responsible for the new mesoporosity observed from physisorption data.

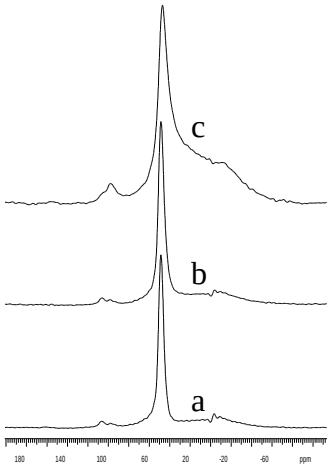

Figure 1. ^{27}Al MAS NMR spectra for (a) NaM, (b) NaMF1, (c) NaMF10 samples.

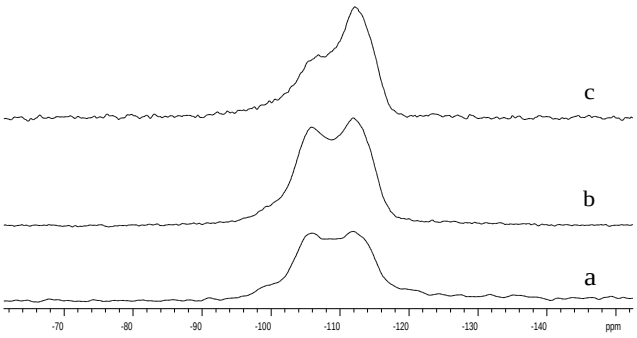

Figure 2. ^{29}Si MAS RMN of (a) NaM, (b) NaM1F and (c) NaM10F.

From the ^{29}Si NMR results (Figure 2), the starting mordenite and the low fluorinated mordenite show three bands at -115 ppm, –105 ppm, and –100 ppm (less intense) which correspond to the Si coordinated to 0 Al, 1 Al and 2 Al, respectively. ^{29}Si NMR spectra for NaM and NaM1F samples are very similar with a very slight decrease of the band at –105 ppm for NaM1F, which indicates a few dealumination not observed before by ^{27}Al NMR. For the NaM10Fsample, this band at –105 ppm tends to disappear, increasing the band at –115 ppm. From these results, we can suggest that the dealumination observed is mainly produced by the initial attack of fluorine to the SiOHAl groups of its acidic form (HM10F).

X-ray powder diffraction patterns of mordenite samples before and after fluorination were taken. The samples, which show similar cristallinity, were identified as mordenite. Additionally, no other phases were detected although the ^{27}Al MAS NMR spectra showed the presence of octahedral aluminum for the highly fluorinated sample (NaM10F), as reported above.

Nevertheless, some structural modifications have been detected as reflected in the variation of the cell parameters calculated from the diffraction patterns (see Table 3). The cell volume practically does not change for the NaM1F sample respect to the non-fluorinated sample (NaM) whereas there is a significant decrease in the cell volume value for the sample NaM10F. However, the cell parameters values do not change in the same direction since parameter *a* increases whereas parameters *b* and *c* decrease when increasing the fluorine treatment. These different tendencies are a consequence of several factors such as the incorporation of fluorine in the structure as well as the dealumination of samples but also the presence of extraframework aluminium in the channels of the mordenite. Therefore, we think that the decrease observed in the cell volume for sample NaM10F should be mainly due to both dealumination and incorporation of the fluorine in the structure.

Table 3. Cell parameters of NaM, NaM1F and NaM10F samples calculated by XRD.

Sample	a (Å)	b (Å)	c (Å)	Cell volume (Å^3)
NaM	18.103(4)	20.451(3)	7.514(1)	2782
NaM1F	18.113(4)	20.437(3)	7.512(1)	2781
NaM10F	18.181(4)	20.383(3)	7.490(1)	2775

In order to confirm this behavior, the IR spectra of HM, HM1F and HM10F samples were also taken. Figure 3 shows the FTIR spectra in the region compressed between 3800 and 3500 cm^{-1}. For the non-fluorinated sample (HM) two peaks are observed at 3740 and 3645 cm^{-1}. The first corresponding to SiOH terminal groups, and the second corresponding to SiOHAl groups although it cannot be discarded the presence of silanol groups related to structural defects.[29] After fluorination, some changes are observed in the FTIR spectra of that region, especially respect to the band at 3645 cm^{-1} since the band at 3740 cm^{-1} does not almost change for both samples. This makes us to think that the attack of fluorine practically does not affect the terminal silanol groups.

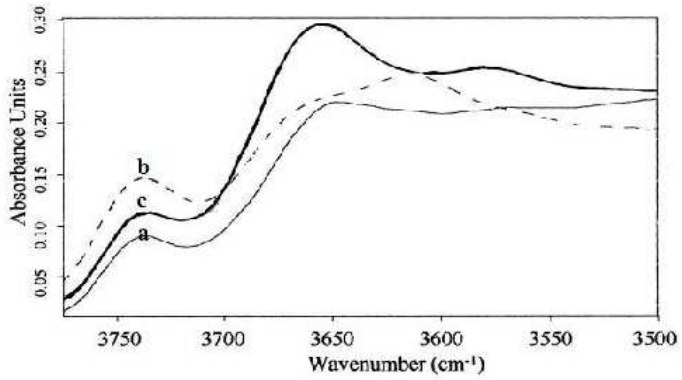

Figure 3. FTIR spectra of (a) HM, (b) HM1F and (c) HM10F samples.

For the HM1F sample, a new band appears at 3614 cm^{-1}. We think that this band corresponds to the same bridged groups of that of 3645 cm^{-1} observed for the non-fluorinated sample. It shifts to lower wavenumber probably due to the effect of the fluorine introduced inside the structure, which makes them more acidic. The shift observed is in agreement with the appearance of framework species (3), previously proposed by Kowalak et al.[23,24]

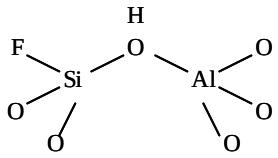

(3)

Also, a less intense band was observed for this sample around 3650 cm^{-1}, which should correspond to the original SiOHAl groups.

For the sample HM10F, more important changes are observed. The first is the appearance of a more intense band at 3655 cm^{-1}. From the results obtained by ^{27}Al MNR for this sample, and together with the data found in the literature,[24] this band can be attributed to AlOH non-framework groups formed as a consequence of the dealumination. Second, there is a band at 3580 cm^{-1} which could be explained in a similar way that the band observed at 3614 cm^{-1} for the HM1F sample. In this case, the higher red shift of the SiOHAl groups band could be due to the presence of stronger Brönsted sites, associated to a more extensive fluorination suffered by NaM10F, although the interaction of these groups with some Al-F species formed during dealumination in the intracrystalline space probably contributes to this shift.[30]

Moreover, the shift in the position for symmetric and asymmetric TO_4 tetrahedra bands in the mid-IR region (see Table 4), is almost the same for the non-fluorinated (NaM) and the low fluorinated (NaM1F) structures, but

shifting towards higher frequencies for the highly fluorinated sample (NaM10F), confirming the dealumination of the structure.

Table 4. IR Frequencies of fluorinated Mordenites, C.E.C. and Si/Al ratio determined by X-ray fluorescence

Sample	IR frequencies (cm^{-1})		C.E.C. (meq/100g)	Si/Al ratio
	ν_{as} (T-O)	ν_{s} (T-O)		
NaM	1064	630	240	7.0
NaMF1	1065	629	217	7.4
NaMF10	1072	637	52	8.2

Finally, to complete the characterization of samples, X-ray fluorescence element maps distribution (not shown here) of Si, Al and Na were also performed and Si/Al ratio was determined by X-ray fluorescence for some samples. Si, Al and Na maps distribution showed an homogeneous atomic distribution in all cases. Quantification results, expressed as Si/total Al (framework + extraframework) ratio (Table 4), indicate that in addition of what was observed by other techniques, there is an initial loss of aluminium during fluorination treatment, which is higher when a higher amount of NH_4F is used. The same tendency was observed in the C.E.C. values (Table 4). The more important decrease observed for the NaM10F sample is in agreement with the presence of extraframework $[Al(OH)_{3-x}]^{x+}$ groups, hardly exchangeable, which are responsible for the neutralization of the framework charge.

3.1.2.2. N_2 and O_2 adsorption measurements.

Nitrogen and oxygen adsorption isotherms are shown in Figures 4, 5 and 6 for different samples. The adsorption volume values are referred to the weight of sample before activation (cm^3/g). The N_2/O_2 selectivity results are listed on

Table 5. N_2/O_2 selectivity was calculated as the ratio between the volume of N_2 adsorbed and the volume of O_2 adsorbed at three given pressures (760, 345 and 50 mmHg).

From the results exhibited in Figure 4 and Table 5, for the non-fluorinated samples it can be observed that substitution of Na^+ cations by Li^+ cations leads to an increase on the adsorption volume and, besides, there is also an increase on the N_2/O_2 adsorption selectivity. This is attributed to the major charge/radium ratio of the Li^+, which favours the electrostatic interaction with the adsorbate molecules.[6]

Table 5. N_2/O_2 adsorption selectivity at 298 K at different pressures.

Sample	Selectivity [a]		
	760 mmHg	**345 mmHg**	**50 mmHg**
NaM	2.8	3.3	4.1
NaMF10	2.0	2.2	2.3
NaMF1	2.8	3.4	4.6
LiM	3.0	4.0	6.6
LiMF1	2.9	4.0	7.2
LiAgM	2.8	4.0	7.3
LiAgMF1	3.0	3.9	6.3
AgM	3.3	4.3	10.2

[a] N_2/O_2 adsorption selectivity was defined as the ratio of the volum adsorbed of N_2 and the volume adsorbed of O_2 at the given pressure

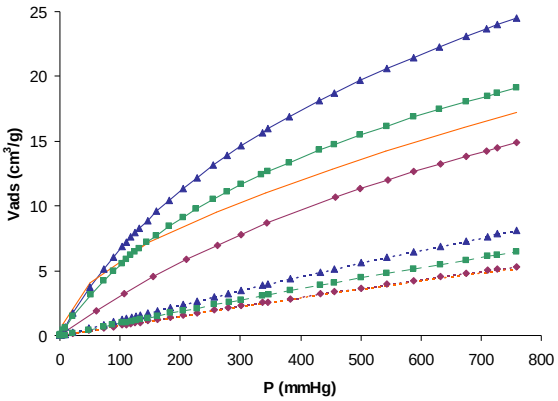

Figure 4. Equilibrium isotherms of N_2 (upper) and O_2 (lower) at 298 K on NaM (♦), LiM (▲),Li/AgM (■) and AgM (—).

Interestingly, the adsorption volumes obtained for these Na-Mordenite and Li-Mordenite samples are slightly higher than those reported in the literature[12] for NaX and LiX samples, respectively, with comparable selectivity values. This reveals the importance of the accessibility of the cations for the gas molecules and confirms our expectations about the use of a zeolite with less cation content but more accessible.

On the other hand, when Na^+ cations are substituted by Ag^+ cations in the mordenite, the isotherm shape becomes less linear (Figure 4). This has also been observed in other Ag-exchanged zeolites,[12] where the N_2/O_2 selectivity increases specially at low pressures. In contrast, we observe a less increase in the total volume adsorbed for the AgM sample respect to the reported for other Ag-exchanged zeolites. This can be attributed to the different degree of complexation interactions, since it is well known that these interactions are strongly influenced by the nature of the zeolite.[31,32]

The adsorption results obtained after the fluorination procedures are shown in Figures 5 and 6 and in Table 5. NaM1F and LiM1F show similar behavior respect to the volume adsorbed and adsorption selectivity results. The total volume adsorbed decreases in both cases after fluorination. This could be explained by a slightly decrease in the number of active sites, because some dealumination takes place when the amount of fluorine introduced is low, according to the Si/Al ratio and C.E.C. values (Table 4). Interestingly, these results also show an increase on selectivity preferentially at low pressures for both samples. This indicates a less shielding of cations when F atoms are incorporated inside the mordenite structure, because of the less polarizability character of fluorine although, probably, fluorination only affects to the more accessible surface.

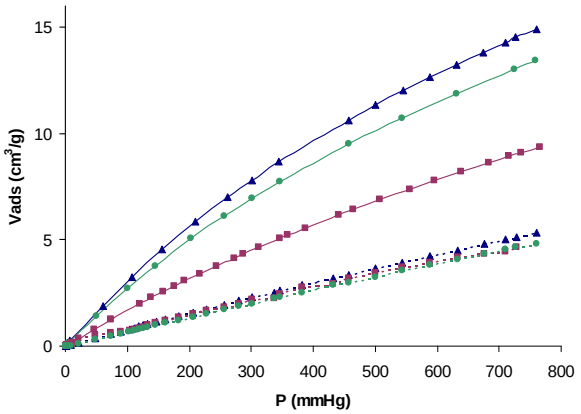

Figure 5. Equilibrium isotherms of N_2 (upper) and O_2 (lower) at 298 K on NaM (■), NaMF1 (●), Na MF10 (▲).

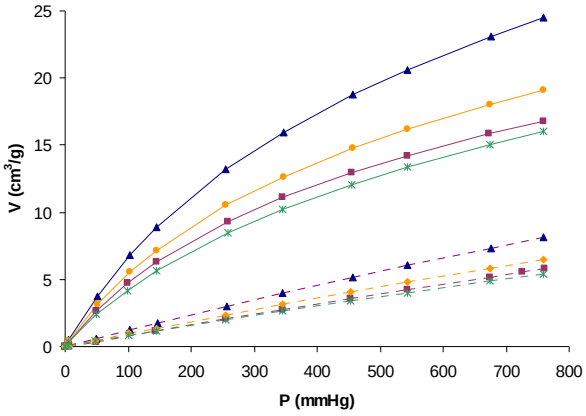

Figure 6. Equilibrium isotherms of N_2 (upper) and O_2 (lower) at 298 K on LiM (▲), LiM1F (■), LiAgM (●), LiAgM1F (×).

On the other hand, for the NaM10F sample, with more fluorine introduced, both volume adsorbed and adsorption selectivity decrease sharply due to the higher dealumination and the presence of hardly exchangeable $[Al(OH)_{3-x}]^{x+}$ groups, which should have scarcely capacity for quadrupolar interaction . This involves a considerable decrease in the number of active sites.

Otherwise, the introduction of small amounts of fluorine in the presence of Ag^+ cations (sample LiAgM1F) results in a decrease both on the volume adsorbed and on the N_2/O_2 selectivity. This can be explained by the effect of the high electronegativity and low polarizability of the fluorine atoms, which cause a decrease on the π-complexation interactions between the cations Ag^+ and the N_2 and O_2 molecules.

In a study reported by Yang et al.[33] about the adsorption of oxygen and nitrogen on silver halides revealed that the polarization effect can influence the 5s orbital energies of Ag. In fact, the difference of energy between the highest occupied molecular orbital (HOMO) of the adsorbate and the lowest

unoccupied molecular orbital (LUMO) of the adsorbent increases when the polarizability of the halide decreases and, consequently, the presence of fluorine probably contributes to obtain a weaker adsorbate-adsorbent interaction, although not important differences between N_2 and O_2 can be expected. However the electronegativity of fluorine atoms would "attract" the electronic density from the Ag and, consequently, this reduces the contribution of backdonation. This reduction affects more to nitrogen since its two π^*-antibonding orbitals are empty while those of oxygen are occupied by one electron each. This explains the decrease in the N_2/O_2 selectivity.

3.1.4. Conclusions

Mordenite, in spite of its Si/Al ratio of 6.5, can adsorb slightly higher volumes of N_2 than zeolites with lower Si/Al ratio, maintaining high N_2/O_2 selectivity. This behaviour can be explained because its 2-dimensional porous structure in channels makes easier the cation accessibility than in zeolites based on cavities. Therefore, this natural zeolite is a good alternative to the synthetic zeolite X for the N_2/O_2 separation process.

In samples prepared by cationic exchange, the volume of N_2 adsorbed increases in the way $Li^+ > Ag^+ > Na^+$ and the adsorption selectivity N_2/O_2 in the way $Ag^+ > Li^+ > Na^+$. For samples exchanged with Li^+ and Na^+ cations, linear isotherms typical of weak electrostatic interaction are observed whereas for Ag^+ samples parabolic isotherms are observed as a consequence of the π-complexation interactions.

The introduction of fluorine in the structure framework is found to have a positive effect on the N_2/O_2 adsorption selectivity. The fluorination with high amounts of NH_4F involves an important dealumination, while the fluorination

with low amounts does not practically cause dealumination of mordenite and some fluorine remains inside the structure modifying the electronic properties of some cations. This fluorine results in a less shielding of these cations by the framework structure, which leads to an increase on the N_2/O_2 selectivity adsorption at lower pressures, despite the loss of the number of active sites.

3.1.5. Acknowledgements

The authors are grateful for the financial support of the Fundación Domingo Martínez and to the Generalitat de Catalunya (2002FI 00667).

3.1.6. References

[1] Sicar, S. *Adsorpt. Sci. Technol.* **2001**, 19, 347.

[2] Kim, J. N.; Chue K. T.; Cho S. H. *Separ. Sci. Technol.* **1995**, 30(3), 347.

[3] Yang, R. T. *Gas separation by adsorption process*; Butterworth: Boston, USA, 1987 reprinted by Imperial College Press, London and World Scientific Publishing Co.: River Edge, NJ, 1997; pp 9-48.

[4] Armor, J. N. Molecular sieves for air separation. In *Materials chemistry: An Emerging Discipline*; Interrante, L. V.; Casper, L. A.; Ellis, A. B. Eds.; ACS: Washington, USA, 1995; pp 321-334.

[5] Ruthven, D. M. *Principles of adsorption and adsorption processes*; John Wiley & Sons, Inc.: New York, USA, 1984.

[6] Coe, C. G., *Acces in Nanoporous Materials*; Pinnavaia, J. B.; Thrope, M. F., Eds.; Plenum Press: New York, 1995.

[7] Coe, C. G.; Kirner, J. F.; Pierantozzi, R.; White, T. R. U.S. Patent 5152813, 1992.

[8] Pápai, I.; Goursot, A.; Fajula, F.; Plee, D.; Weber J. *J. Phys. Chem.* **1995**, 99, 12925.

[9] Rege, S. U.; Yang, R. T. *Ind. Eng. Chem Res.* **1997**, 36, 5358.

[10] Chousdary, V. N.; Jasra, R. V.; Bhat, T. S. Ind. Eng. Chem Res. **1993**, 32, 548.

[11] Chao, C. C. EP Patent 0297542A2, 1998.

[12] Yang, R. T.; Chen, Y. D.; Peck, J. D.; Chen, N. *Ind. Eng. Chem. Res.* **1996**, 35, 3093.

[13] Smudde, G. H.; Slager, T. L.; Coe, C. G.; MacDougall, J. E.; Weigel, S. J. *Appl. Spectrosc.* **1995**, 49 (12), 1747.

[14] Kazansky, V. B.; Bülow, M.; Tichomirova, E. *Adsorption* **2001**, 7, 291.

[15] Goursot, A.; Vasilyev, V.; Arbuznikov, A. *J. Phys. Chem. B* **1997**, 101, 6420.

[16] Shen, D.; Bülow, M.; Jale, S. R.; Fitch, F. R.; Ojo, A. F. *Micropor. Mesopor. Mat.* **2001**, 48, 211.

[17] Kazansky, V. B. *J. Mol. Catal. A: Chem.* **1999**, 141, 83.

[18] Jale, S. R.; Búlow, M.; Fitch, F. R.; Perelman, N.; Shen, D. *J. Phys. Chem. B* **2000**, 104, 5272.

[19] Jasra, R. V.; Choudary, N. V.; Bhat, S. G. T. *Ind. Eng. Chem. Res.* **1996**, 35, 4221.

[20] Panov, A. G.; Gruver, V.; Fripiat, J. *J. Catal.* **1997**, 168, 321.

[21] Sánchez, N. A.; Saniger, J. M.; d'Epinose de la Caillerie, J. B.; Blumenfeld, A. L.; Fripiat, J. *J. Catal.* **2001**, 201, 80.

[22] Belzunce, M. J.; Mendioroz S.; Haber, J. *Clay. Clay Miner.* **1998**, 46 (6), 603.

[23] Becker, K. A.; Kowalak, S. *J. Chem.Soc., Faraday Trans I* **1985**, 81, 1161.

[24] Kowalak, S.; Khodakov, A. Y.; Kustov, L. M.; Kazanky, V. B. *J. Chem. Soc. Faraday Trans.* **1995**, 91(2), 385.

[25] Breck, D. W.; Skeels, G. W. in *Proc. 6th Int. Congr. Catal. (The Chemical Society, London, 1977)*, vol 2, p. 645.

[26] Bergaya, F.; Vayer, M. *Appl. Clay Sci.* **1997**, 12, 275.

[27] Hutson, N. D.; Zajic, S. C.; Yang, R. T. *Ind. Eng. Chem. Res.* **2000**,39, 1775.

[28] Gregg, S. J.; Sing, K. S. W. *Adsorption, surface area and porosity*; Academic Press: London, UK, 1982.

[29] Jentys, A.; Lercher, J. A. Tecniques of zeolite characterization. In *Introduction to zeolite science and practice*; van Bekkum, H.; Flanigen, E. M.; Jacobs, P. A.; Jansen, J. C. Eds.; Elsevier: Amsterdam, NL, 2001. pp 345-386.

[30] Becker, K. A.; Kowalak, S. *J.Chem.Soc, Faraday Trans.I* **1986**, 82, 2157.

[31] Wu, Z.; Han, S.; Cho, S.; Kim, J.; Chue, K.; Yang, R. T. *Ind. Eng. Chem. Res*, **1997**, 36, 2749.

[32] Safark, D. J.; Eldridge, B. *Ind. Eng. Chem. Res.* **1998**,37, 2571.

[33] Chen N.; Yang, R. T. *Ind. Eng. Chem. Res.* **1996**, 35, 4020.

3.2. Influence of the Ag^+ location on the N_2 and O_2 adsorption properties of several Na/Ag-A zeolites

Abstract

Two silver A zeolites were prepared from Na-A zeolite by cation exchange using different Ag^+ concentration. The samples were activated at different temperatures under vacuum in order to study the evolution of their N_2 and O_2 adsorption properties. X-ray diffraction and UV-visible Diffuse Reflectance techniques were used for samples characterization. Adsorption and characterization results showed that the location of Ag^+ cations on/in the zeolite A structure plays an important role on its adsorption properties. Thus, when very low Ag^+ concentration was used for sample preparation, Ag^+ cations are mainly located on the external surface and during vacuum-temperature activation, silver metallic particles are formed, which partially block the entrance to the gas molecules, decreasing the N_2 and O_2 adsorption volumes with a slight decrease of the N_2/O_2 adsorption selectivity respect to Na-A. For the sample exchanged with higher Ag^+ concentration, Ag^+ cations are located inside the cavities of the zeolite. The different samples obtained by the application of temperature under vacuum show higher N_2 and O_2 adsorption volumes respect to the zeolite Na-A, due to their stronger interaction with the silver cations, showing the maximum N_2/O_2 selectivity and the highest N_2 adsorbed volume at 623 K. Surprisingly, when the activation temperature increases over that value, there is a decrease of the N_2 adsorbed volume while the O_2 adsorbed volume increases which could be associated to the migration-reduction of some Ag^+ cations with the temperature.

3.2.1. Introduction

Zeolites, since their first application reported by Barrer,[1] have been mainly used at industrial and laboratory level as catalysts, cation exchangers and selective adsorbents due to their shape selectivity and acidic properties.[2] However, for air separation, shape selectivity at room temperature is not the discriminating feature, since N_2 and O_2 have similar molecular size, but separation depends on the structure type of the zeolite and the number, type, degree of hydration, and location of the extraframework cations.[3,4] Thus, small structural modifications can induce strong modifications in their adsorption behaviour.[5]

Zeolite structures that contain Ag^+ cations as extraframework cations have been extensively used as adsorbents for paraffin/olefin separations on the basis of π-complexation,[6,7] and also, catalysts containing both Ag^o and Ag^+ are important in partial oxidation processes.[8] Silver cations can also interact with N_2 and O_2 molecules by π-complexation, where the bond has two contributions: the donation of π-bond electrons of the N_2 and O_2 molecules to the empty s-orbital of Ag^+, and the backdonation of the d-orbital electrons of Ag^+ (4d orbitals filled with 10 electrons) to the empty antibonding π orbitals of the molecules.[9] This second contribution is lower for O_2 molecules since the antibonding π orbitals are partially occupied on O_2 molecules.

According to the studies published by Yang et al., X and LSX zeolites containing Ag^+ showed N_2 and O_2 adsorption properties that could be related to the presence of silver clusters (Ag_m^{n+}) inside the zeolite, which seem to favor the interaction with the nitrogen molecules, increasing the N_2/O_2 adsorption selectivity.[9,10] The formation of these clusters has been investigated for different zeolites (zeolite A, X, Y and LSX) by several authors which reported that when dehydration takes place, by applying temperature and/or vacuum, two different phenomena could be observed: first, silver cations can interact with other near

silver cations, and second, Ag^+ cations can interact with framework oxygen giving an autorreductive process in suitable conditions, where the transition metal reduces and water or lattice oxygen oxidates.[11] The nuclearity and charge of the clusters formed is certainly dependent on the pretreatment conditions used.[12-17]

Although we can find in the literature many studies about the silver clusters formation within zeolite A, there are only few studies about the adsorption of N_2 and O_2 using this Ag^+ modified zeolite.[18,19] In these studies, an improvement of N_2 adsorption properties, respect to the zeolite Na-A, was observed when fully Ag^+-exchanged commercial zeolite A was activated at temperatures between 623 and 653 K. The good adsorption results published for this commercial zeolite show the interest of its use for the N_2/O_2 separation. However, it is not easy to explain this behavior. Sebastián et al.[18] pointed out that a strong interaction with Ag_m^{n+} species or with the wall charge generated in typical Ag^+ autoreductive processes together with the migration of Ag^+ cations from α to β cavities could explain those results. This let us to think that more studies are needed in order to try to understand that behavior.

The aim of this work is to study the influence of the silver species location on the N_2 and O_2 adsorption properties at room temperature of several silver A zeolites, prepared by treatment of NaA zeolite with two different $AgNO_3$ concentrations. In order to induce variations on the cation distribution in the zeolite structure, the samples were activated at different temperatures under vacuum.

3.2.2. Experimental Section

3.2.2.1. Starting materials

The starting material of this work is a commercial Na-A zeolite (Si/Al = 1) supplied by Prolabo as hydrated binderless pellets with chemical composition 1 Na_2O : 1 Al_2O_3 : 2 ± 0.1 SiO_2 : xH_2O. Silver nitrate ($AgNO_3$, > 99.8 %, Prolabo) was used for samples preparation.

3.2.2.2. Samples preparation

Commercial zeolite was treated in a mortar until a fine powder was obtained. Then, two samples were prepared by cation exchange with different $AgNO_3$ concentration. The one was prepared using higher concentration of silver cations than the other.

Samples Na/Ag(1M)-A and Na/Ag(0.01M)-A were prepared by exchanging at room temperature under stirring for 48 h, 2 g and 0.5 g of zeolite Na-A with 33 mL of $AgNO_3$ 1M and 0.01M, respectively. These experiments were carried out completely protected from light in order to avoid the reduction of Ag^+ cations to metallic silver. Afterwards, the samples were filtered and washed with abundant distilled water and finally dried at 383 K overnight.

3.2.2.3. Characterization techniques

Samples were characterized by powder X- ray diffraction, and UV-Visible Diffuse Reflectance.

Powder X-ray diffraction. (XRD). High Temperature XRD measurements were obtained with a Siemens D5000 diffractometer (Bragg-Brentano parafocusing

geometry and vertical θ-θ goniometer) equipped with an Anton-Paar HTK10 platinum ribbon heating stage. The angular 2θ diffraction range was between 5º and 70º and the measuring time per degree was 6 sec. Ni-filtered $Cu_{K\alpha}$ radiation (30 mA, 40 kV) and a Braun position sensitive detector (PSD) were used. The patterns were collected at 298, 573, 623, 673 and 723 K and at heating rate of 5 K/min. A static argon-atmosphere was used throughout the measurement. The crystalline phases were identified using the Joint Committee on Powder Diffraction Standards (JCPDS) files. The JCPDS files used were 75-2484 and 4-0783 for the zeolite and metallic Ag phases, respectively. From the diffraction patterns, the deconvolutions and cell parameter calculations for each phase ere made using the TOPAS 2.1 software by Brücker-AXS in which the instrument error is corrected.

UV-Visible Diffuse Reflectance. Experiments were performed on a Shimadzu UV-2101 UPC equipment. Spectra were recorded in the range 200 nm to 800 nm at room temperature.

N_2 and O_2 adsorption measurements. Adsorption isotherms were measured using a static volumetric system Micromeritics ASAP-2010. The gases used were high purity (99.999%) N_2 and O_2. Both gases were supplied by Carburos Metálicos.

Adsorption experiments were made using an amount of sample between 0.2 to 0.3 g. Sample was contained in a quartz cup and previously activated before the adsorption measurements at different temperatures (623 K, 673 K, 723 K (for 3 h), 723 K (for 8 h) and 723 K (for 15 h)) using a turbo molecular vacuum pump until a pressure lower than 1 μmHg since it is known that small amounts of molecular water inside the framework of the aluminosilicates seriously affect the adsorption capacity of these materials.[4] Adsorption measurement of pure N_2 and pure O_2 were performed separately at 298 K in the range of pressures compressed between 0.05 and 760 mmHg. The adsorption volume values are

referred to the weight of sample before activation (cm^3/g). N_2/O_2 selectivity was calculated as the ratio between the adsorbed volumes of each pure gas at 760 mmHg.

3.2.3. Results and Discussion

3.2.3.1. Samples characterization

Figure 1 shows the X-ray diffraction patterns of the Na/Ag(1M)-A and Na-A samples. The cristallinity of the zeolite does not vary significantly after exchange, as observed.

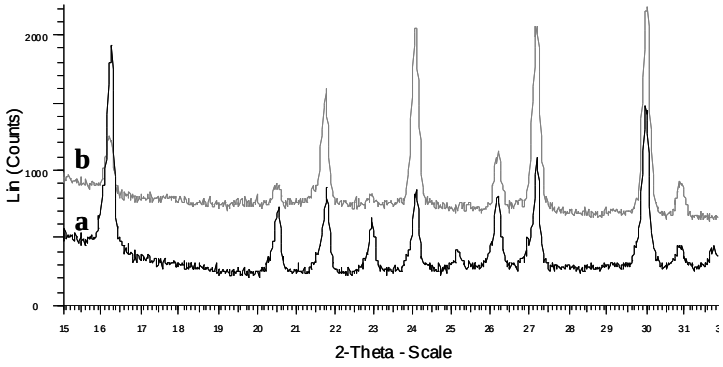

Figure 1. X-ray diffraction patterns of the samples a) Na/Ag(1M)A, and b) NaA.

Table 1 shows the different colors observed for the samples after the activation treatment depending on the conditions used. Sample Na/Ag(1M)-A shows a wider variety of colors than the sample Na/Ag(0.01M)-A.

Table 1. Colors observed after the activation treatment for both samples.

Sample / T^a (K)	573	623	673	723 (3h)	723 (8h)	723 (15h)
Na/Ag(1M)-A	Yellow	Orange	Redish	Redish	Brown	Dark-brown
Na/Ag(0.01M)-A	Greyish	Blackish	Metallic-black	Metallic-black	-	-

In order to follow the possible formation of different silver species, which could explain the different colors observed, several powder X-ray diffraction experiments were performed using a temperature chamber.

The X-ray diffraction patterns obtained for sample Na/Ag(0.01M)-A (Figure 2A) show the peaks corresponding to the zeolite Na-A. Additionally, a new peak seems to appear at 2θ equal to 38.1 at temperatures higher than 623 K, which corresponds to the (100) peak of metallic silver associated with the cubic crystallographic Fm3m group (indicated on the figure). The deconvolution of these diffractograms confirms the presence of metallic Ag particles. One example of XRD deconvolution is given in Figure 2B for the sample cooled at 298 K after the sample was activated at the different temperatures.

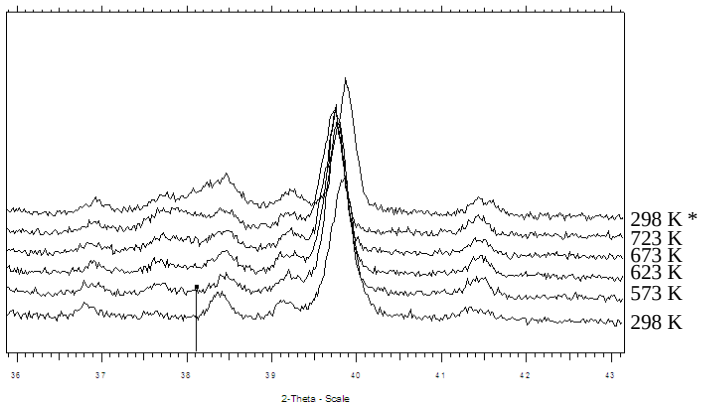

Figure 2A. XRD of Na/Ag(0.01M)-A sample at 298, 573, 623, 673, 723 and 298* K. The diffraction line at 2θ=38,1 corresponds to the (100) Ag Fm3m (JCPDS file). * this XRD pattern was taken after cooling at 298 K the sample previously activated at the different temperatures.

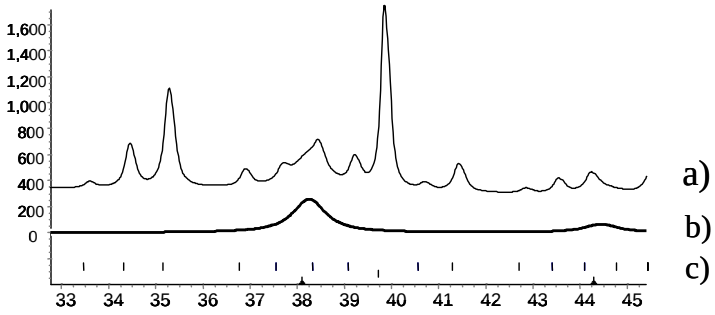

Figure 2B. Whole powder pattern decomposition a) XRD pattern of sample Na/Ag(0.01M)-A cooled at 298 K after the sample was activated at the different temperatures; b) Pattern obtained by subtracting the A zeolite JCPDS file to the pattern a); c) A zeolite diffraction lines (JCPDS file).

The structure of the zeolite Na-A corresponds to the cubic $Pm\bar{3}m$ group and its cell parameter is 11.9735 Å. Table 2 shows the cell parameters of the zeolite and Ag particles calculated from the XRD patterns of sample Na/Ag(0.01M)-A at the different temperatures. As we can see, the cell parameter of the zeolite almost does not change with the temperature. Only a small increase was observed at temperatures higher than 298 K due to the unit cell expansion, which could indicate a low Ag^+ cations exchange degree. However, the adsorption of some Ag^+ on the external surface could explain the presence of metallic particles. Ag^+ cations on the surface can easily migrate and form bigger aggregations giving to the formation of the detected metallic silver particles, whose cristallinity and size increases by increasing the temperature. This is in agreement with the black color observed for this sample at temperatures higher than 623 K (Table 1).

Table 2. Zeolite and Ag cell parameters for the activated Na/Ag(0.01M)-A samples.

Sample	T[a] (K)	Cell parameter (zeolite, Å)	Cell parameter (Ag, Å)
Na/Ag(0.01M)-A	298	11.9705(1)	-
	573	11.9760(3)	-
	623	11.9799(2)	4.1155(1)
	673	11.9844(1)	4.1182(5)
	723	11.9875(4)	4.1249(3)
	298*	11.9670(1)	4.0876(1)

* This sample was cooled at 298 K after it was activated at the different temperatures

The behaviour observed for this Na/Ag(0.01M)-A sample is quite different with respect to other previously reported when exchanging a pure synthesized zeolite A at low silver loading.[14,16,20] In those publications, the authors only observe cationic exchange phenomena. The fact that we use to prepare sample

Na/Ag(0.01M)-A a very low $AgNO_3$ concentration together with the use of a commercial zeolite A (which can contain impurities traces) could explain a certain adsorption of Ag species on the external surface.

On the other hand, no peak due to metallic silver was detected by X-ray diffraction for the Na/Ag(1M)-A sample at any temperature. This is in agreement with the color variation observed for this sample. Also, the cell parameter of that zeolite increases up to 12.3572 Å. This increase is indicative that, in this case, Ag^+ cations are located in the internal positions, and consequently, the unit cell expands maintaining the same symmetry when the Na^+ cations are replaced by the bigger Ag^+. Despite the different colors observed, which could be related to the presence of different Ag_m^{n+} species, it was not possible to detect them by this technique.

In order to characterize those Ag_m^{n+} species, UV-Visible spectra of Na/Ag(1M)-A sample treated at different temperatures were also taken and the spectra were compared with others described on the literature. In this kind of AgA materials, some typical bands, due to charge transferences from the oxygen of the zeolite walls to silver cations, can be observed for this kind of samples in the range compressed between 400 and 600 nm depending on the cation coordination:[15,20] a) the absorption band at 420 nm, caused by the presence of Ag^+ cations in a 6 or 8 O-rings sites; b) the absorption band at 475 nm, only visible when the Ag^+ cations occupy the 4-ring oxygen sites, responsible for the yellow colour; and c) the absorption band at 530 nm when a Ag^+ cation located in a 4-ring oxygen has a second Ag^+ as a neighbor, responsible for the red color.

Table 3 indicates the UV-visible bands for the Na/Ag(1M)-A samples. Observing these data, the sample treated at 298 K shows an intense band at 404 nm, which can be attributed to the type-a) transition. This sample also shows a band at 470 nm associated to the type-b) transition. The samples treated at 573

K and 673 K show also two bands associated to the type a) and b) transitions. However, a progressive increase of the band corresponding to the transition type b) at expenses of the band associated to the transition type a) was observed when increasing temperature. This indicates some migration of silver cations from 6 or 8 O-rings sites to 4 O-ring sites when higher temperatures are used. Finally, for the samples treated at 723 K for different times (3 h, 8 h and 15 h) major changes can be observed. The first and the second spectra show an intense band around 475 nm whereas the band around 420 nm appears just like a small shoulder, indicating a very low amount of silver cations in 6 and 8 O-rings sites for these samples. Otherwise, the UV-Vis spectrum of the third sample, treated at 723 K for 15 h, is completely different. A new band appears at 554 nm, which can be associated to the presence of Ag_m^{n+} species. Although this band could not be observed for the other samples activated at higher temperatures than 673 K, these Ag_m^{n+} species should be present, in small amounts, as suggests the color observed for these samples.

Tabla 3. Absorption wavenumber in nm of the different transitions observed on the UV-Vis region for the Na/Ag(1M)-A sample.

Temperature (K)	a) transition	b) transition	c) transition
298	404	470	-
573	411	463	-
673	417	466	-
723(3h)	420*	477	-
723 (8h)	412*	472	-
723 (15h)	-	-	554

*shoulder

3.2.3.2. N_2 and O_2 adsorption measurements.

The N_2 and O_2 adsorption results are shown in Figures 3 and 4 for the samples Na/Ag(0.01M)-A and Na/Ag(1M)-A, respectively. For the Na/Ag(0.01M)-A sample, all the isotherms (N_2 and O_2) obtained show a linear tendency and lower gas adsorbed volumes than the Na-A zeolite. Otherwise, for the Na/Ag(1M)-A samples, O_2 isotherms show also a linear tendency, while for N_2 isotherms a more parabolic tendency can be observed in comparison with the Na-A sample. This parabolic tendency has been related to the strong π-complexation interactions of the silver cations with the N_2 molecules.[9] In this case, the adsorbed volumes of both gases are higher for the Na/Ag(1M)-A samples than for the Na-A zeolite.

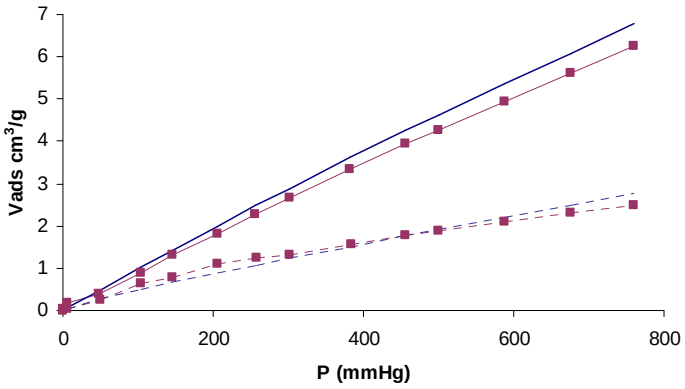

Figure 3. Equilibrium isotherms of N_2 (—) and O_2 (---) at 298 K on the samples Na/Ag(0.01M)-A (■) and Na-A (no symbol) activated at 673 K.

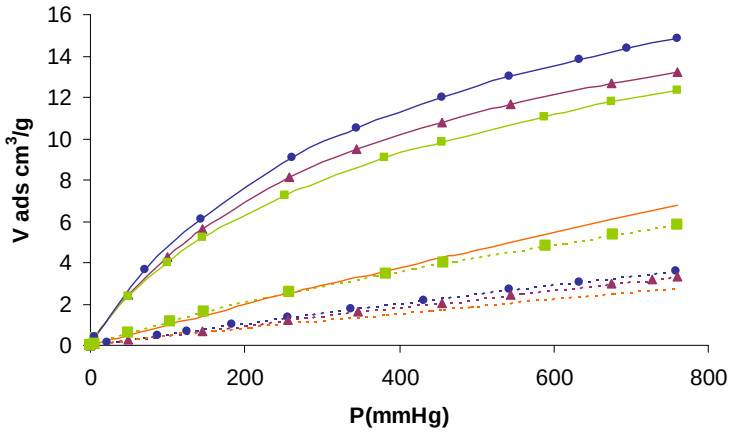

Figure 4. Equilibrium isotherms of N_2 (▬) and O_2 (---) at 298 K on Na/Ag(1M)A activated at different temperatures: 623K (●), 673K (▲), 723 K (■) comparing with Na-A zeolite (no symbol).

Regarding sample Na/Ag(0.01M)-A, we observe that when it is activated, in order to eliminate all the water located inside the cavities, it becomes blackish from 623 K (Table 1). Thus, the observed decrease of the N_2 and O_2 adsorbed volumes together with the slight decrease of the N_2/O_2 adsorption selectivity respect to the Na-A sample (Figure 3) can be associated to the formation of silver metallic particles on the zeolite external surface, which become more crystalline at higher temperatures, according to the XRD characterization results. The presence of these particles hinders the access of the gas molecules, since they partially block the entrance of the cavities, and consequently, the number of adsorbed molecules decreases. The linearity observed for these isotherms is also in agreement with the XRD results that showed very low amounts of Ag^+ inside the cavities for this sample, since the zeolite cell parameter almost does not change respect to the Na-A zeolite (Table 2). This explains the slight decrease of N_2/O_2 selectivity values observed for sample

Na/Ag(0.01M)-A with respect to the Na-A sample (Figure 3) since silver cations do not participate on the interaction with the gas molecules.

On the other hand, for the Na/Ag(1M)-A samples, the volume of adsorbed N_2 and O_2 is always higher than for the Na-A sample independently of the different activation temperature used (Figure 4). This can be mainly explained in terms of the higher $\Delta H_{adsorption}$ of N_2 and O_2 values obtained for silver zeolites than for sodium zeolites.[9]

Interestingly, as we can see numerically in Table 4, this sample presents the maximum adsorbed volume of N_2 at 623 K, which starts to decrease when temperatures higher than 673 K are used in the activation process. Respect to the adsorbed O_2 volume, it is always lower than the N_2 adsorbed volume at all activation temperatures tested. On the other hand, it is surprising that the volume of adsorbed O_2 decreases from 623 K to 673 K, whereas for activation temperatures higher than 673 K, the total O_2 adsorbed volume increases. In outline, N_2/O_2 adsorption selectivity decreases when higher temperatures than 623 K are used in the activation process.

Table 4. N_2 and O_2 adsorbed volumes (in cm^3/g) and N_2/O_2 adsorption selectivity at 760 mmHg for the Na/Ag(1M)-A sample activated at different temperatures.

Temp (K)	Vads N_2	Vads O_2	N_2/O_2 Selectivity
623	14.83	3.59	4.13
673	13.55	3.35	3.95
723 (3 h)	12.35	5.84	2.11

We think that in order to understand this behavior, the cation location in the zeolite plays an important role. In a fully silver exchanged zeolite A, eight cations are located at 6 O-rings, one cation is located at 4 O-ring, and three

silver cations at 8 O-rings, which are mainly related with the diffusion trough the channels.[14] By applying temperature, the cations located in the 8 O-rings probably move towards inside the framework and possibly toward the β-cages (6 O- and 4 O-rings). These migration processes are usually accompanied by an autoreduction process: this means that some silver cations reduce to Ag^0 atoms and, framework oxygen or water oxygen oxidate. When the activation temperature increases, this autoreduction is favored and an increase in the number of Ag^0 atoms can be expected. The main consequences would be: a) an increase of the N_2 and O_2 adsorbed volumes at moderated temperatures due to the migration of cations located in the mouth of the channels (8 O-rings), which favor the access of the N_2 and O_2 molecules into the cavities, and b) a decrease on the N_2 adsorbed volume at higher temperatures because the cations located in the 4 O-rings are less accessible for the gas molecules and also, due to a more important decrease on the number of Ag^+ cations associated to some reduction process. In this way, at higher temperatures we can also explain the observed increase on the O_2 adsorption volume, since silver atoms present more affinity for O_2 than N_2.[21] The increase of the number of Ag atoms at these higher activation temperatures justifies the dark color observed at 723 K (Table 1).

Although in the activation process positive charges are generated on the structural walls and silver aggregations (Ag_m^{n+}) are formed,[18] both with potential ability to interact selectively with N_2 respect to O_2 molecules, from our results, we think that the main responsible for the adsorption properties of these silver cation-exchanged A zeolite samples is the accessibility of the molecules to the Ag^+ species together with the presence of Ag atoms, since the increase of the number of positive defects on the walls and the bigger silver aggregations species (Ag_m^{n+}) formed by increasing the activation temperature cannot explain the decrease of the N_2/O_2 selectivity observed.

3.2.4. Conclusions

The main conclusion that we can extract from our work is that the N_2 and O_2 adsorption capacity of silver cation exchanged commercial A zeolite is greatly affected by the silver concentration on sample preparation and also by the conditions under which these samples are activated.

Thus, sample (Na/Ag(0.01M)-A) presents lower adsorption capacity than Na-A zeolite because during the sample activation process, silver metallic particles are formed, which partially hinder the entrance of the gas molecules to the cavities of the zeolite. On the other hand, the sample prepared using higher amounts of Ag^+ cations (Na/Ag(1M)-A) shows higher adsorption capacity than Na-A with a maximum N_2/O_2 selectivity at 623 K. This can be explained because the Ag^+ cations located in the 8 O-ring sites can migrate to more internal sites, and consequently the accessibility of the molecules to the cations is more favored. However, at higher activation temperatures, an increase of the O_2 adsorbed volume together with a decrease of the N_2 adsorbed volume was observed for this Na/Ag(1M)-A sample. In this case, besides the migration, some cations reduce to Ag^0 atoms. The presence of Ag^0 atoms, which have tendency to interact with O_2 molecules, and the loss of silver cations justify this behavior.

The results presented in this paper show the good N_2/O_2 separation properties of the fully exchanged commercial Ag-A zeolite when using the appropriated activation conditions.

3.2.5. Acknowledgements

The authors are grateful for the financial support of the Fundación Domingo Martínez and to the Generalitat de Catalunya (2002FI 00667).

3.2.6. References

[1] Barrer, R. M. *J. Soc. Chem. Ind.* **1945,** 64, 130.

[2] Yang, R. T. *Gas separation by adsorption process*; Butterworth: Boston, USA, 1987 reprinted by Imperial College Press, London and World Scientific Publishing Co.: River Edge, NJ, 1997.

[3] Choudary, V. N.; Jasra, R. V.; Bhat, T. S. G. *Ind. Eng. Chem. Res.* **1993**, 32, 548.

[4] Hutson, N. D.; Zajic, S. C.; Yang, R. T. *Ind. Eng. Chem. Res.* **2000**, 39, 1775.

[5] Coe, C. G. In Gas separation technology: proceedings of the International Symposium on Gas Separation Technology, Vasant, E. F.; Dewolfs, R. (Eds.), Elsevier, 1990, p. 149.

[6] Safarik, D. J.; Eldridge, R. B. *Ind. Eng. Chem. Res.* **1998**, 37, 2571.

[7] Huang, H. Y.; Padin, J.; Yang, R. T. *J. Phys. Chem.* **1999**, 103, 3206.

[8] Choi, E. Y.; Kim, S. Y.; Kim, Y.; Seff, K. *Micropor. Mesopor. Mater.* **2003,** 62, 201.

[9] Yang, R. T.; Chen, Y. D.; Peck, J. D.; Chen, N. *Ind. Eng. Chem. Res.* **1996**, 35, 3093.

[10] Hutson, N. D.; Reisner, B. A.; Yang, R. T.; Toby, B. H. *Chem. Mater.* **2000**, 12, 3020.

[11] Jacobs, P. A.; Uytterhoeven, J. B.; Beyer, H. K. *J. Chem. Soc.*, Faraday Trans. **1979**, 75, 56.

[12] Kim, Y.; Sep, K. *J. Am. Chem. Soc.* **1978**, 100, 175.

[13] Gellens, L. R.; Mortier, W. J.; Schoonheydt, R. A.; Uytterhoeven, J. B. *J. Phys. Chem.* **1981**, 85, 2783.

[14] Seifert, R.; Rytz, R.; Calzaferri, G. *J. Phys Chem. A* **2000**, 104, 7473.

[15] Miyanaga, T.; Hoshino, H.; Endo, H. *J. Synchrotron Rad.* **2001**, 8, 557.

[16] Calzaferri, G.; Leiggener, C.; Glaus, S.; Schürch, D.; Kuge, K. *Chem. Soc. Rev.* **2003**, 32, 29.

[17] Pavlovskaya, G. A.; Horton-Garcia, C. F.; Dybowski, C.; Corbin, D. R.; Meersmann, T. *J. Phys. Chem. B* **2004**, 108, 1584.

[18] Sebastián, J.; Jasra, R. V. *Chem. Comm.* **2003**, 268.

[19] Sebastián, J.; Jasra, R. V.; *UK Paten, GB 2386889*, 2003.

[20] Seifert, R.; Kunzmann, A.; Calzaferri, G. *Angew. Chem. Int. Ed.* 37 **1998,** 11, 1521.

[21] Pazzi, V. I.; Philipsen, P. H. T.; Baerends, E. J.; Tantardini, G. F. *Surf. Sci.* **1999**, 443 (1-2), 1.